OPEN ACCESS
JOURNAL OF ADVANCED DIELECTRICS
Vol. 12, No. 5 (2022) 2250019 (7 pages)

DOI: 10.1142/S2010135X22500199

Colossal dielectric response and complex impedance analysis of $LaFeO_3$ ceramics

Sushrisangita Sahoo[*,‡], K. P. Andryushin[*], P. K. Mahapatra[†] and R. N. P. Choudhary[†]

[*]*Research Institute of Physics, Southern Federal University*
344090, Rostov-on-Don, Russia

[†]*Department of Physics, Siksha O Anusandhan (Deemed to be University)*
Bhubaneswar, India

[‡]sushri1990@gmail.com

Received 9 June 2022; Revised 25 August 2022; Accepted 21 September 2022; Published 8 November 2022

The present investigations mainly focused on the colossal dielectric response and complex impedance analysis of $LaFeO_3$ ceramics. The studied sample was prepared by a citrate gel method. Structural and microstructural properties are analyzed from the XRD pattern and SEM micrograph. The anomalies in the dielectric constant versus temperature plots are analyzed on the basis of polarization induced by the Maxwell–Wagner mechanisms and ferromagnetic interaction between the Fe^{3+} ions driven by the oxygen vacancy mediated Fe^{3+}–V_o–Fe^{3+} exchange interaction A giant dielectric permittivity in the order of ~10^5 was observed in the sample even at the room temperature for 100 Hz. The colossal dielectric constant in $LaFeO_3$ is mainly driven by the internal barrier layer capacitor (IBLC) formation. The formation of IBLC was explained on the basis of highly insulating grain boundary and less resistive/semiconducting grain, which was confirmed from both the resistance and capacitance of grain and grain boundary from the impedance analysis. The non-Debye-type relaxation process associated with the grain and grain boundary effect was investigated from the broad and asymmetric relaxation peak. The relaxation time for both the grain and grain boundary effect was also calculated. In addition to this, we have also analyzed the normalized bode plot of imaginary part of impedance and electrical modulus which suggests the relaxation process dominated by the short-range movement of charge carriers.

Keywords: Ferrite; giant dielectric constant; non-Debye; relaxation.

1. Introduction

Development of novel materials with colossal dielectric response became a main research hub of the contemporary material researchers due to its potentiality in many microelectronics applications such as multilayer capacitors, high energy density storage devices, integrated passive components for microelectronics, etc. There are many excellent colossal dielectric permittivity materials such as doped $BaTiO_3$, $CaCu_3Ti_4O_{12}$ (CCTO), doped NiO_5, $Bi_{0.5}Na_{0.5}TiO_3$, $Ni_{0.5}Zn_{0.5}Fe_2O_4$, ZnO_8 etc., but the high permittivity of the ferroelectric materials, such as $BaTiO_3$ and (K, Na) NbO_3, can only be attained over a narrow temperature range close to the ferroelectric phase transition. The stronger temperature dependence limits their applications.[1–5] The dielectric loss of other nonferroelectric materials with colossal values of ε is too high in the application point of view. The main focus of the scientific society in these classes of materials is to understand the fundamental mechanism of the colossal dielectric permittivity and to develop new material with enhanced material characteristics. Lanthanum Ferrite ($LaFeO_3$) is one such material exhibiting giant dielectric permittivity along with other fascinating properties like catalytic and gas sensing behavior, magnetic properties, multiferroic properties, etc. $LaFeO_3$ was widely studied as catalyst for the decomposition of hydrocarbons, chlorinated volatile organic compounds (VOCs) or by the reaction between NO and CO. It is also used as photo-catalysts and catalysts in heterogeneous Fenton-like reactions for the wet peroxide oxidation of hydrocarbons. In addition to this, lanthanum orthoferrites and doped $LaFeO_3$ (A-site and/or B-site substituted) are also investigated as sensor materials for the detection of humidity, alcohol, oxygen, etc. and as electrode materials in Solid Oxide Fuel Cells (SOFCs). Multiferroic properties of $LaFeO_3$ was also reported by Bhargav *et al*.[6–9] Though lanthanum ferrite is widely investigated for catalytic and electrodes of SOFC purpose, the dielectric and electrical properties of lanthanum ferrite still need an extensive investigation.

So, in this present endeavor, we tried to explore the reason behind the colossal dielectric response of lanthanum ferrite in the wide temperature due to three dielectric anomalies and electrical heterogeneity. A comprehensive study was also carried out to verify the electrical heterogeneity of the sample responsible for the colossal dielectric permittivity through the complex impedance analysis. The relaxation process corresponding to grain and grain boundary was broadly

‡Corresponding author.

analyzed on the basis of complex impedance spectroscopy and electrical modulus study.

2. Materials and Methods

$LaFeO_3$ ceramic sample was synthesized by citrate gel method. High purity lanthanum oxide La_2O_3, ferric nitrate nonahydrate Fe $(NO_3)_3.9H_2O$ and citric acid ($C_6H_8O_7$) were taken as precursor materials for synthesis of $LaFeO_3$ ceramics. The detailed procedure was illustrated through flow diagram in Fig. 1. The stoichiometric amount of the individual solution of La_2O_3, Fe $(NO_3)_3.9H_2O$ and $C_6H_8O_7$ is mixed through continuous magnetic stirring along with temperature at around 70–80°C for 6–7 h to obtain a homogenous nitrate-citrate solution. The viscous nitrate–citrate solution was heated at 100°C at oven overnight and a porous crunchy mass was then obtained. The porous crunchy mass was crushed and grounded to fine powder with a mortar pestle. The fine powder was then placed on alumina crucible and calcined at 700°C. After phase confirmation of the calcined powder from the room temperature XRD data, the calcined powders were pressed to form pellets of cylindrical shape with varying dimensions (Diameter: 12 mm and thickness:1–3 mm).

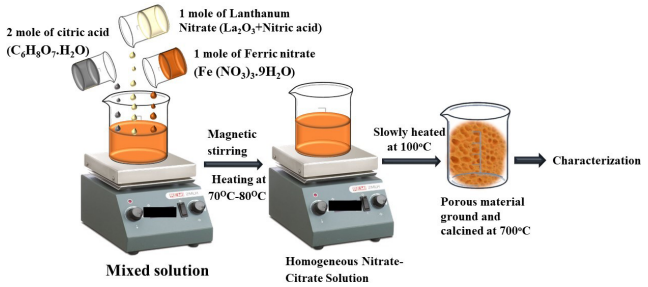

Fig. 1. Schematic representation of $LaFeO_3$ fabrication by citrate gel method.

The pellets are then sintered at 1200°C for 4 h. These sintered pellets are then used for dielectric and electrical (impedance and conductivity) measurement (using Phase sensitive meter, PSM 1735, N4L) after electroding with silver paste. Such technology, among other things, can cause texturing of the grain landscape and, as a result, improve the properties of the final product (increase in density, etc.). Microstructure (i.e., surface micrograph) and EDS spectrum (for compositional analysis) of the sintered pellets were obtained from a scanning electron microscope (SEM, FEI, QUANTA-250).

3. Results and Discussions

The indexed XRD spectrum of the chemically synthesized $LaFeO_3$ sample is shown in Fig. 2(a). The XRD spectrum of our prepared sample matched well with standard crystal data of lanthanum orthoferrites ((as illustrates through blue stick pattern, JCPDS no. 01-088-0641) with orthorhombic crystal structure. The lattice parameters of the sample were found to be a = 5.5707 Å, b = 7.8561 Å and c = 5.5585 Å. The crystallite size (D) and the lattice strain (ε) of the prepared sample were calculated from the Williamson–Hall plot (as shown in Fig. 2(b)) on the basis of Williamson–Hall Equation as follows[10]:

$$\beta\cos\theta = K\lambda + 4\varepsilon\sin\theta, \tag{1}$$

where $K = 0.9$ is the shape factor and λ is the wavelength of the CuKα radiation. The crystallite size and the lattice strain are found to be 52.72 nm and 0.00206, respectively.

The surface micrograph and the EDS pattern of the investigated sample are shown in Fig. 3. The polycrystalline nature of the sample is clearly observed from the distinguished grains separated by the grain boundaries. Some pores are observed in the microstructure. The grain size and distribution of grains are analyzed from the histogram (as shown in the inset of the SEM image). The average grain size of the

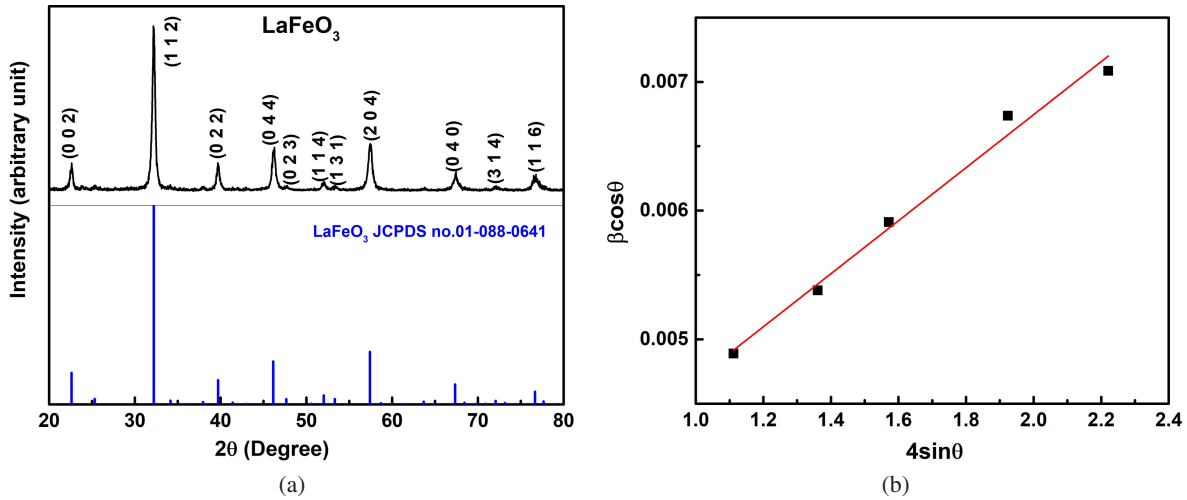

(a) (b)

Fig. 2. (a) XRD pattern with standard crystal data of $LaFeO_3$ ceramics (b) Williamson–Hall plot.

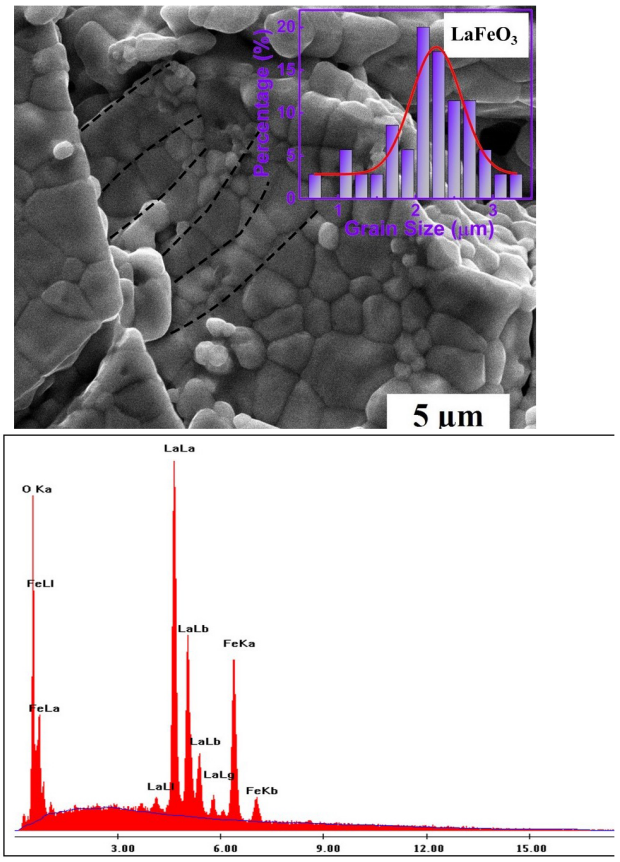

Fig. 3. SEM image, histogram (in the inset of SEM micrograph) and EDS spectra of $LaFeO_3$ ceramics.

sample is 2.26 μm. The EDS pattern does not exhibit any other elements than the expected elements (La, Fe and O) suggesting the absence of impurity element in the material. However, it should be noted that in Fig. 3, which illustrates a fragment of the grain landscape of the material, texturing elements are predicted in the form of "columns" of close-packed grains (framed by dashed lines in Fig. 3). Attention is drawn to the fact of a certain discreteness of such textured regions, which may be associated with the features of the formation of the microstructure of this particular composition.

Figure 4 shows both the temperature and frequency-dependent behavior of $LaFeO_3$. We observed three anomalies at around 50°C, 140°C and 230°C for 500 Hz–10 kHz frequency in the ε_r versus temperature plot. But, the two anomalies at around 50°C and 140°C merge together and a broad peak appears for the frequency above 10 kHz as depicted in the corresponding inset of the figure. The clear insight of the three anomalies is also illustrated through the fitting of experimental data with the three Gaussian peaks. Similar trend with two dielectric anomalies at around 50°C and 150°C was also reported in the literature[11,12] in the temperature-dependent ε_r characteristics of $LaFeO_3$. Further, from the literature survey, we found that $LaFeO_3$ shows the colossal dielectric constant value (~10^4–10^5) even below the transition temperature.[9,13]

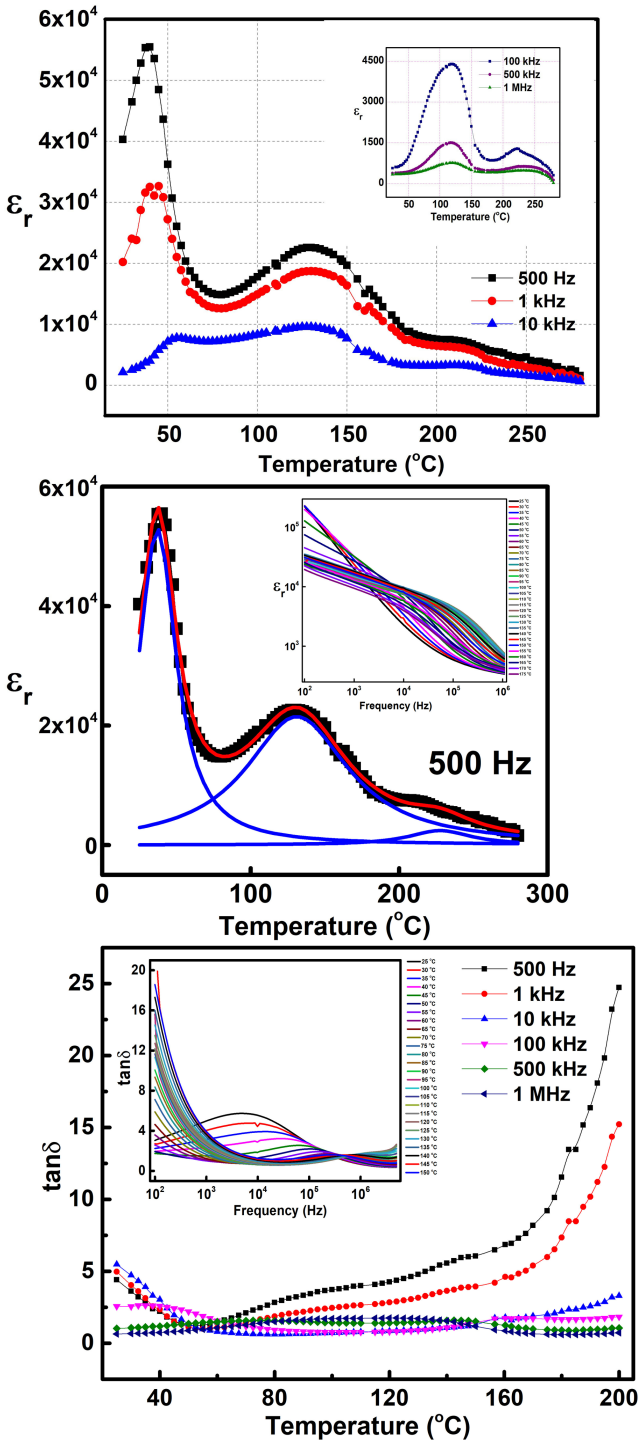

Fig. 4. Variation of ε_r and tanδ with temperature and frequency (in the inset).

Bhargav *et al.*[12] reported a large value of dielectric constant to the tune of 21,000 at 1 kHz frequency at around 140°C. In our experimental result, we observed that the amplitude of the first peak is higher than that of the second anomaly at lower frequency. With the increase in frequency, the amplitude of the first peak decreases and finally disappears at

higher frequency. From these features, we analyzed that the dielectric polarization is associated with the anomaly around 50°C which shift to the higher temperature with an increase in frequency that has the characteristics of Maxwell–Wagner mechanism.

According to this mechanism, a material consists of a highly resistive grain boundary and less resistive grain resulting in an internal barrier layer capacitor and yields giant dielectric constant. This explanation can later be verified from the analysis of Nyquist plot. The second anomaly at around 150°C is associated with the polarization induced from the grain capacitance due to some extrinsic effect. This peak is being observed by many authors,[11,12] but has not been assigned for any reason behind the occurrence of the peak.

As we know, the Maxwell–Wagner mechanism is effective only at lower frequency, above 10 kHz, the peak was absent. The colossal or giant dielectric value at low temperature and low frequency is mainly due to extrinsic effect. The giant dielectric constant due to IBLC formation can also be realized from the step like response corresponding to the grain boundary effect in the ε_r versus frequency plot. The anomaly at higher temperature, i.e., around 230°C is associated with the dielectric polarization induced from the ferromagnetic interaction between the Fe^{3+} ions driven by the oxygen vacancy mediated Fe^{3+}–V_o–Fe^{3+} exchange interaction. The lanthanum ferrite sample exhibits a similar trend of dielectric material in the temperature variation of tanδ i.e., the increase in value of tanδ with temperature due to increase in conductivity. The frequency-dependent variation of tanδ reveals about the relaxation process of the material, which was comprehensively investigated in our earlier report.[14]

Complex Impedance Spectroscopy is a very significant technique to explore the electrical characteristics of polycrystalline materials (mostly ceramics) and its correlation with the microstructural characteristics. By virtue of this technique, one can differentiate the contributions of intrinsic grain (or bulk) and extrinsic grain boundaries. The physical mechanism associated with the material can be represented by an appropriate equivalent circuit network. The circuit networks corresponding to grain and grain boundary are generally constituted capacitances 'C' (since our materials are dielectric materials) and resistances 'R' (due to loss associated with

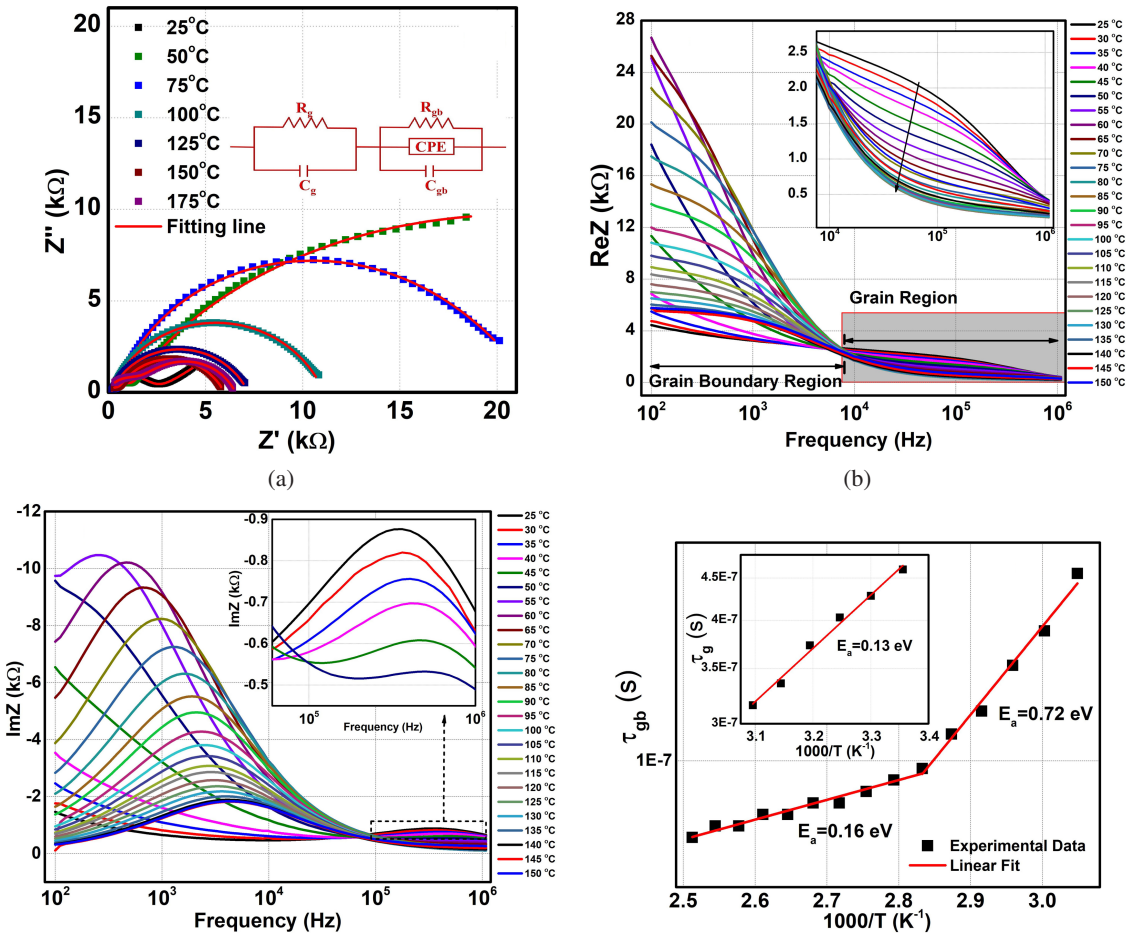

Fig. 5. (a) Nyquist plot, (b) ReZ versus frequency, (c) ImZ versus frequency, (d) Relaxation time of grain and grain boundary versus inverse temperature.

the capacitor). The intrinsic grain and extrinsic grain boundary effects in complex impedance plot (also called as Nyquist plot) emerged in the shape of successive semicircular arc. The nature of the semicircular arc (i.e., perfect or depressed) specifies the relaxation mechanisms (Debye or Non-Debye) of the samples. Perfect semicircular arc (i.e., center on real *Z*-axis) specifies the Debye type relaxation mechanism, while the depressed one (center below the real *Z*-axis) indicates the non-Debye relaxation process. The former, each semicircle can be represented by a parallel RC network signifying the *dc* conduction mechanism (*R*) in parallel with the dielectric polarization (*C*); whereas for the latter one, a constant phase element (*Q*) was included parallel to the RC circuit network. But, a series combination of two parallel RC circuits is considered where the grain boundary is adjacent to a grain (conducting or semiconducting). In this case, the grain boundary (the barrier depleted of charge carriers) appears as a capacitance, while the grain looks like a series resistance.[15,16] The effect of intrinsic grain and extrinsic grain boundary on the electrical characteristics of our studied sample was illustrated through the complex impedance plot in Fig. 5(a). The experimental complex impedance plot was fitted with suitable circuit network (as specified in the inset of Fig. 5(a)) using Zsimpwin software.

The inclusion of *Q* in the circuit model indicates the non-Debye-type relaxation mechanisms. The grain and grain boundary effects are clearly visible in the plot. The first semicircle (in high frequency region) indicates the intrinsic grain contribution and the second semicircle (in lower frequency region) indicates the extrinsic grain boundary effect.

The resistances and capacitances of grain (R_g and C_g) and grain boundary (R_{gb} and C_{gb}) at some selected temperatures (25°C, 50°C, 75°C, 100°C, 125°C, 150°C and 175°C) are tabulated in Table 1. From the table, it is clear that the grain boundary resistance is much more than the grain resistance indicating the conducting grains with blocking grain boundaries. Due to the blocking (or highly resistive) grain boundaries, charge carriers are accumulated; which acts as a capacitor with high value of capacitance than the intrinsic grain. The grain and grain boundary resistance (after 65°C) decreases with increase in temperature indicating the NTCR behavior of the sample.

Table 1. Grain and grain boundary resistances and capacitances at various temperatures.

Temperature (°C)	R_g (Ω)	C_g (F)	R_{gb} (Ω)	C_{gb} (F)
25	2.149×10^3	1.083×10^{-6}	7.311×10^3	1.447×10^{-10}
50	8.759×10^2	2.244×10^{-10}	3.703×10^4	8.702×10^{-10}
75	3.710×10^2	2.117×10^{-10}	2.053×10^4	1.557×10^{-8}
100	2.007×10^2	1.946×10^{-10}	1.090×10^4	9.406×10^{-9}
125	1.701×10^2	1.909×10^{-10}	7.026×10^3	6.243×10^{-9}
150	4.114×10^2	2.732×10^{-10}	5.6×10^3	4.471×10^{-9}
175	2.2×10^3	1.219×10^{-8}	5.046×10^3	1.403×10^{-9}

The variations of real and imaginary parts of impedance (i.e., ReZ and ImZ, respectively) with frequency at some selected temperatures are illustrated in Figs. 5(b) and 5(c). These plots are important to study the resistive characteristics and relaxation process of the sample. The effect of intrinsic grain and extrinsic grain boundary is also observed in these plots, i.e., the results can be correlated with the Nyquist plot. The low-frequency region indicates the grain boundary characteristics whereas the high-frequency region suggests the grain characteristics, as indicated in Fig. 5(b). The enlarged version of the grain region was also shown in the inset of the figure. The enhanced value of Z' at lower frequency region was due to the higher value of grain boundary resistance. As observed in the Nyquist plot (listed in Table 1), the grain boundary resistance is maximum for 50°C and then decreases with a rise in the temperature. This characteristic was also found in the Z' versus frequency plot i.e., the grain boundary resistance increases up to 65°C and then decreases with an increase in the temperature. Similarly, the decrease in grain resistance with a rise in the temperature also confirmed here similar to that of Nyquist plot indicating the semiconducting nature of the sample. The relaxation peak observed in ImZ versus frequency plot in lower and higher frequency region indicates the effect of extrinsic grain boundary and intrinsic grain, respectively. Thermally activated relaxation process was predicted from the shifting of relaxation peak with an increase in the temperature. The broad and asymmetric peak for both the grain and grain boundary again confirmed the non-Debye relaxation process. The characteristics parameter i.e., the relaxation time (τ) for the relaxation process corresponding to the grain and grain boundary effect was calculated from the relation $\omega\tau = 1$ (at the relaxation peak) and plotted with the variation of inverse temperature as illustrated in Fig. 5(d). The τ_{gb} versus inverse absolute temperature exhibits two distinct slopes at two different temperature regions indicating the different relaxation mechanism associated with the studied material. The activation energy for both the slopes was calculated on the basis of Arrhenius relation[17]:

$$\tau = \tau_0 \exp(-E_a/(k_B T)), \quad (1)$$

and found to be 0.16 eV and 0.72 eV for high-temperature and low-temperature region, respectively.

Similarly, the activation energy for the grain effect was found to be 0.13 eV. The decrease in relaxation time with increase in temperature for both the grain and grain boundary effect is attributed to the increase in the hopping rate of thermally activated charge carriers. In addition to the complex impedance spectra for the understanding of grain and grain boundary relaxation process, we have also plotted the frequency-dependent plot of electrical modulus. Electrical modulus provides a clear vision to the less capacitive and resistive grain interior which was suppressed in the complex impedance plot due to more resistive grain boundary.

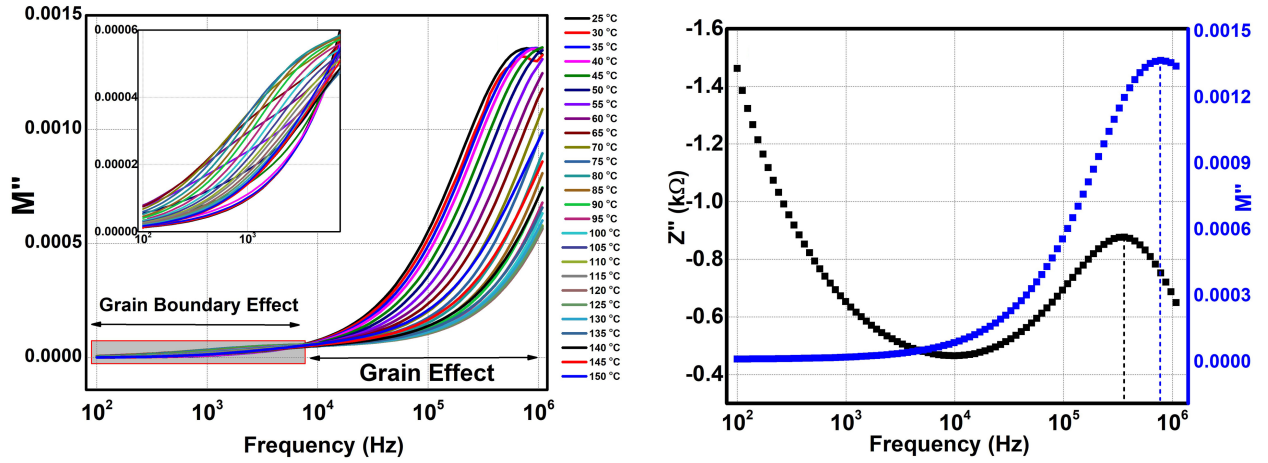

(a) (b)

Fig. 6. (a) Imaginary part of modulus versus frequency and (b) normalized Bode plot.

The relaxation process corresponding to the grain is now prominently visible in the high-frequency region of the imaginary plot of electrical modulus (M″) versus frequency (Fig. 6(a)). The relaxation peak corresponding to the grain effect shifted to higher frequency range (beyond our experimental studied range) and only observed for few temperatures up to 35°C. The normalized bode plot (ImZ and M″ versus frequency) at room temperature was plotted to explore whether the relaxation process is associated with the short-range or long-range movement of charge carriers. If the relaxation peak of both the ImZ (Fig. 6(b)) and M″ versus frequency coincides, then it indicates that the long-range movement of charge carriers is responsible for the relaxation process, otherwise, if the two have separate characteristic frequency, then the relaxation process was dominated by the short-range movement of charge carriers.[18] In our study, the relaxation peak for both the bode plot observed at different frequency suggested the relaxation process to get associated with the short range movement of the charge carriers.

4. Conclusions

$LaFeO_3$ ceramic was synthesized by a low-temperature and cost-effective method i.e., citrate gel method. The phase formation of the synthesized material was confirmed from the room temperature XRD pattern and the observed pattern matches well with the JCPDS data. The preliminary structural analysis reveals the sample crystallizes in an orthorhombic structure. The crystallite size and lattice strain of the studied sample was calculated using Williamson–Hall plot and found to be 52.72 nm and 0.00206, respectively. The anomalies in the dielectric constant versus temperature plots are attributed to the polarization induced by the Maxwell–Wagner mechanisms and ferromagnetic interaction between the Fe^{3+} ions driven by the oxygen vacancy mediated Fe^{3+}–V_o–Fe^{3+} exchange interaction. A giant dielectric permittivity was observed in the sample due to the formation of internal barrier layer capacitor as a consequence of highly insulating grain boundary and less resistive/semiconducting grain. The electrical heterogeneity of the sample was also confirmed from the complex impedance and electrical modulus analysis. The non-Debye type relaxation process associated with the grain and grain boundary effect was analyzed and correlated with all the analysis of complex impedance and modulus i.e., Nyquist plot, real and imaginary part of impedance, and the imaginary part of modulus.

Lanthanum orthoferrite exhibiting colossal dielectric constant has promising applications in on-chip capacitors and Dynamic Random Access Memory (DRAM) devices. The studied material i.e., Lanthanum orthoferrites also have applications in humidity sensors, oxygen sensors, etc.

Acknowledgments

Sushrisangita Sahoo would like to thank Dr. M. L. Nandagoswami, Department of Physics, Midnapore College for his kind help in some experimental work.

The study was financially supported by the Ministry of Science and Higher Education of the Russian Federation (State task in the field of scientific activity, scientific project No. (0852-2020-0032)/(BAZ0110/20-3-07IF).

This report was presented at the 10th Anniversary International Conference on "Physics and Mechanics of New Materials and Their Applications" (PHENMA 2021), Divnomorsk, Russia, May 23–27, 2022.

References

[1]X. Liu, H. Fan, J. Shi and Q. Li, Origin of anomalous giant dielectric performance in novel perovskite: $Bi_{0.5-x}La_xNa_{0.5-x}Li_xTi_{1-y}M_yO_3$ ($M = Mg^{2+}$, Ga^{3+}), *Sci. Rep.* **5**, 12699 (2015).

[2]P. Lunkenheimer, V. Bobnar, A. V. Pronin, A. I. Ritus, A. A. Volkov and A. Loidl, Origin of apparent colossal dielectric constants, *Phys. Rev. B* **66**, 052105 (2002).

[3]Y.-Q. Tan, Y. Meng and Y.-M. Hao, Structure and colossal dielectric permittivity of Ca_2TiCrO_6 ceramics, *J. Phys. D. Appl. Phys.* **46**, 015303 (2013).
[4]K. Meeporn, T. Yamwong and P. Thongbai, $La_{1.7}Sr_{0.3}NiO_4$ nanocrystalline powders prepared by a combustion method using urea as fuel: Preparation, characterization, and their bulk colossal dielectric constants, *Jpn. J. Appl. Phys.* **53**, 06JF01 (2014).
[5]D. Xu, K. He, B. Chen, C. Xu, S. Mu, L. Jiao, X. Sun and Y. Yang, Microstructure and electric characteristics of $AETiO_3$ (AE=Mg, Ca, Sr) doped $CaCu_3Ti_4O_{12}$ thin films prepared by the sol–gel method, *Prog. Nat. Sci. Mater. Int.* **25**, 399 (2015).
[6]R. Köferstein and S. G. Ebbinghaus, Synthesis and characterization of nano-$LaFeO_3$ powders by a soft-chemistry method and corresponding ceramics, *Solid State Ion.* **231**, 43 (2013).
[7]A. E. Giannakas, A. K. Ladavos and P. J. Pomonis, Preparation, characterization and investigation of catalytic activity for NO+CO reaction of $LaMnO_3$ and $LaFeO_3$perovskites prepared via microemulsion method, *Appl. Catal. B. Environ.* **49**, 147 (2004).
[8]Z. X. Wei, Y. Q. Xu, H. Y. Liu and C. W. Hu, Preparation and catalytic activities of $LaFeO_3$ and Fe_2O_3 for HMX thermal decomposition, *J. Hazard. Mater.* **165**, 1056 (2009).
[9]M. Idrees, M. Nadeem, M. Atif, M. Siddique, M. Mehmood and M. M. Hassan, Origin of colossal dielectric response in $LaFeO_3$, *Acta Mater.* **59**, 1338 (2011).
[10]Y. T. Prabhu, K. V. Rao, V. S. S. Kumar and B. S. Kumari, X-Ray analysis by Williamson-Hall and size-strain plot methods of ZnO nanoparticles with fuel variation, *W. J. Nanosci. Eng.* **4**, 21 (2014).
[11]K. K. Bhargav, S. Ram and S. B. Majumder, Small polaron conduction in lead modified lanthanum ferrite ceramics, *J. Alloys Compd.* **638**, 334 (2015).
[12]K. K. Bhargav, S. Ram and S. B. Majumder, Physics of the multi-functionality of lanthanum ferrite ceramics, *J. Appl. Phys.* **115**, 204109 (2014).
[13]S. Acharya, J. Mondal, S. Ghosh, S. K. Roy and P. K. Chakrabarti, Multiferroic behavior of lanthanum orthoferrite ($LaFeO_3$), *Mater. Lett*. **64**, 415 (2010).
[14] N. Pradhani, S. Sahoo, P. K. Mahapatra and R. N. P. Choudhary, Resolution of loss tangent to grain and grain boundary relaxation and conductivity components, *AIP Conf. Proc.* **2115**, 030013 (2019).
[15]E. Barsoukov and J. Ross Macdonald, *Impedance Spectroscopy Theory, Experiment, and Applications*, 2nd edn. (A John Wiley & Sons, Inc.) (2005).
[16]S. Sahoo, P. K. Mahapatra and R. N. P. Choudhary, Colossal dielectric response, relaxation mechanism and multiferroic properties of $(Ba_{1-x}Sm_x)(Ti_{1-x}Fe_x)O_3$ ($0.0=x=0.5$), *Mater. Sci. Eng. B* **260**, 114624 (2020).
[17]S. Sahoo, P. K. Mahapatra and R. N. P. Choudhary, The structural, electrical and magnetoelectric properties of soft-chemically synthesized $SmFeO_3$ ceramics, *J. Phys. D Appl. Phys.* **49**, 035302 (2016).
[18]M. Coskun, O. Polat, F. M. Coskun, Z. Durmus¸ M. Çaglar and A. Turuta, The electrical modulus and other dielectric properties by the impedance spectroscopy of $LaCrO_3$ and $LaCr_{0.90}Ir_{0.10}O_3$ perovskites, *RSC Adv.* **8**, 4634 (2018).